Ancillary Service Provision and Multi-market Participation of a Cement Plant under Uncertainty

Bruno Laurini, Alessandro Quattrociocchi, Chresten Træholt, Yi Zong
Department of Wind and Energy Systems
Technical University of Denmark
Kongens Lyngby, Denmark
brulau@dtu.dk

Shanmugam Perumal
Green Innovation
FLSmidth Pvt Ltd
Chennai, India
shanmugam.perumal@flsmidth.com

***Abstract*—Industrial demand response is emerging as a key strategy to help balance power systems with increasing levels of variable renewable generation. In particular, cement plants are highly electricity-intensive and can provide demand response through process scheduling and participation in ancillary-service markets. However, taking advantage of this flexibility to reduce operational costs is challenging due to uncertainty in electricity prices, reserve activation, and renewable generation. To address this challenge, this paper develops a multi-stage stochastic optimization model that co-optimizes energy and reserve procurement for a cement plant. A rolling-horizon simulation with out-of-sample evaluation compares performance against deterministic and perfect foresight approaches, demonstrating the value of stochastic methods in managing industrial energy flexibility.**

***Index Terms*—Ancillary services, demand response, stochastic programming, cement plant.**

I. Introduction

The growing penetration of variable renewable generation (RG) has intensified the need for demand-side flexibility to support system reliability, grid stability, and efficient renewable integration. Industry, which is the largest electricity-consuming sector, plays a crucial role in providing such flexibility through demand response (DR). The potential for DR depends on process characteristics such as notification lead time, response speed, and mode of power modulation [1], [2].

Cement production represents a promising industrial DR application due to its combination of high electricity use and intermediate material inventories that partially decouple material and power flows. Previous studies have primarily explored heuristic or mixed-integer linear programming (MILP)–based scheduling strategies to reduce energy costs and peak demand under conventional tariff structures such as time-of-use pricing [3]–[5]. However, only a few have investigated multi-market participation of a cement plant under uncertainty. For instance, [6] proposed a production-inventory MILP that jointly optimizes day-ahead (DA) energy procurement and secondary reserve commitments, while [7] examined manual frequency restoration reserve (mFRR) provision by a Spanish cement plant through an annual DR service auction using a medium-term stochastic model. Nevertheless, short-term operational scheduling considering repeated mFRR activations and cumulative inventory effects remains a research gap.

ECoClay (Project No. 64021-7009) is partially funded by EUDP.

This paper contributes to the development of a stochastic MILP framework for the short-term co-optimization of energy and reserve capacity in a cement plant, explicitly accounting for activation uncertainty and inventory dynamics. A rolling-horizon simulation framework is employed to capture the cumulative impact of repeated reserve activations on both energy use and material inventories. Such a framework is particularly important in markets where reserve capacity is procured on a daily basis (e.g., in the Nordic region), as repeated activations can gradually disturb production schedules and storage levels. Furthermore, because policies derived from historical data may diverge from actual realizations, out-of-sample rolling-horizon simulations are performed to quantify the performance gap against deterministic and perfect-foresight benchmarks. The analysis considers two European reserve products in the DK1 bidding zone (West Denmark): Frequency containment reserve (FCR), supplied by an on-site battery energy storage system (BESS), and mFRR, particularly up-regulation, provided by the cement mill, as the plant's largest schedulable load.

The paper is organized as follows. Section II provides the problem description, outlining the context of cement manufacturing, the decision-making process, and the key modelling assumptions. Moreover, it also describes the multi-stage stochastic optimisation framework, the treatment of uncertainty, and the rolling-horizon simulation procedure. Section III reports the results and discussion, analysing the impacts of ancillary services on production-inventory management, and economic performance. Finally, Section IV summarises the main conclusions of the research and future work.

II. Problem formulation

Cement production involves a sequence of mechanical and thermal processes connected by intermediate inventories that buffer material flows. The process typically begins with quarrying and crushing raw materials into rock-sized fragments. Further size reduction occurs in the raw mill, whose output feeds the main thermal pyroprocessing stage, typically comprising a preheater tower and rotary kiln. In this stage, limestone is calcined and clinker is formed in the kiln. Finally, clinker is cooled and ground in cement mills together with additives, resulting in the final cement blend. In this study, calcined clay—produced in a parallel, electrified

979-8-3315-8138-1

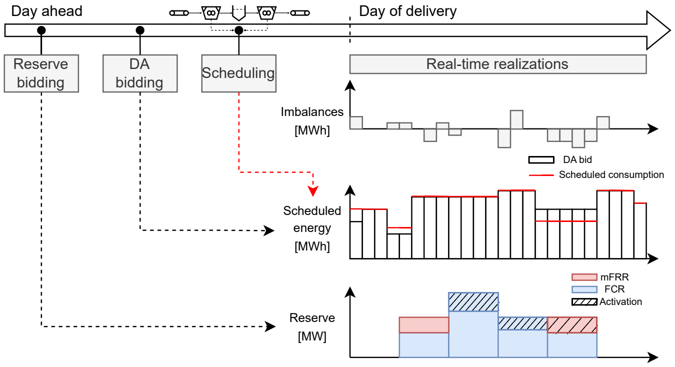

Fig. 1. Decision-making framework for the cement plant, showing market participation and dispatchable processes. Note that imbalances are not necessarily the difference between DA bid and the scheduled consumption, as they are affected by real-time BESS operation and RG uncertainty.

line—is ground with clinker to produce Limestone Calcined Clay Cement (LC3), assumed to contain 50% clinker, 30% calcined clay, 15% limestone, and 5% gypsum [8].

A. Assumptions

Due to thermal and process constraints, the kiln and clay calcination system operate continuously, while the crusher, raw mill, and cement mill are dispatchable on a daily basis. Among these, the cement mill is assumed capable of providing mFRR by deviating from its baseline. On-site RG and BESS support the plant's total load, while the latter can also provide FCR, leveraging its fast power modulation.

The plant is modelled as a balance responsible party (BRP) and price-taker in the Nordic electricity markets. It is financially responsible for real-time deviations between its market position and actual consumption. Operational decisions are structured across multiple markets and timescales, as illustrated in Fig. 1: (i) reserve capacity bidding for FCR and mFRR on day D–1 morning, (ii) energy procurement in the day-ahead market after reserve prices are known, (iii) intraday scheduling of production and inventory, and (iv) real-time adjustments based on realized prices, RG, and activation signals. Given the sequential and uncertain nature of this multi-stage process, the overall problem is formulated as a multi-stage stochastic MILP. Uncertainty is represented through scenario indices $\omega \in \Omega_\omega$, and non-anticipativity constraints ensure consistent decision-making across stages.

B. Objective function

The proposed stochastic MILP minimizes Eq. (1), which includes expected market cost and penalties across all scenarios. The symbol λ denotes either (i) market prices for energy and reserve products, indicated by superscripts, or (ii) penalty weights applied to slack variables. The symbol δ denotes nonnegative slack variables used to relax limits or targets. The first two terms of Eq. (1) represent revenues from FCR and mFRR capacity provision. The third term accounts for mFRR activation energy settled at the activation price. The following three terms reflect day-ahead energy purchases, balancing cost, and imbalance penalty. The last two terms penalize inventory target deviations and violations of the minimum state of charge (SOC) headroom required for FCR delivery.

$$\begin{aligned}\Phi = \sum_{\omega\in\Omega_\omega} \pi_\omega \Bigg(& -\sum_{t\in T}\sum_{b\in B} P^{\text{R,FCR}}_{b,t,\omega}\lambda^{R,FCR}_{t,\omega} \\ & - \sum_{t\in T}\sum_{m\in M} P^{\text{R,mFRR}}_{m,t,\omega}\lambda^{R,mFRR}_{t,\omega} - \sum_{t\in T}\sum_{m\in M}(P^{\text{act,mFRR}}_{m,t,\omega}\Delta t)\lambda^{\text{act,mFRR}}_{t,\omega} \\ & + \sum_{t\in T}(P^{DA}_{t,\omega}\Delta t)\lambda^{DA}_{t,\omega} + \sum_{t\in T}(\Delta P^{\updownarrow}_{t,\omega}\Delta t)\lambda^{RT}_{t,\omega} + \sum_{t\in T}(\Delta P^{I}_{t,\omega}\Delta t)\lambda^{I} \\ & + \lambda^{M}(\delta^{\text{M,+}}_{s,\omega} + \delta^{\text{M,-}}_{s,\omega}) + \lambda^{SOC}(\delta^{\text{SOC,+}}_{b,t,\omega} + \delta^{\text{SOC,-}}_{b,t,\omega}) \Bigg) \end{aligned} \tag{1}$$

C. Constraints

Reserve capacity procurement represents the first-stage decision, where both FCR and mFRR bids must be submitted under activation and price uncertainty.

$$\underline{P}^{\text{R,mFRR}} x^{\text{R,mFRR}}_{t,\omega} \le \sum_{m\in M} P^{\text{R,mFRR}}_{m,t,\omega} \le \overline{P}^{\text{R,mFRR}} x^{\text{R,mFRR}}_{t,\omega} \qquad \forall t\in T, \forall \omega\in\Omega_\omega \tag{2}$$

$$\underline{P}^{\text{R,FCR}} x^{\text{R,FCR}}_{t,\omega} \le \sum_{b\in B} P^{\text{R,FCR}}_{b,t,\omega} \le \overline{P}^{\text{R,FCR}} x^{\text{R,FCR}}_{t,\omega} \qquad \forall t\in T, \forall \omega\in\Omega_\omega \tag{3}$$

These constraints use binary variables $x^{\text{R,FCR}}$ and $x^{\text{R,mFRR}}$, to bound the total reserve capacities offered for mFRR and FCR within regulatory minimum requirements ($\underline{P}^{\text{R,mFRR}}$ and $\underline{P}^{\text{R,FCR}}$) and the sum of available physical capability of each asset m and BESS b ($\overline{P}^{\text{R,mFRR}}$ and $\overline{P}^{\text{R,FCR}}$).

Energy procurement is modelled through constraints that capture the difference between real-time power consumption and day-ahead commitments. DA bidding occurs in the second stage, after reserve capacity prices are realized but before DA prices are known, while real-time (RT) consumption decisions are made in the final stage once all uncertainties are revealed. Constraints (4)-(6) define the signed ($\Delta P^{\updownarrow}_{t,\omega}$) and unsigned ($\Delta P^{I}_{t,\omega}$) power imbalances and ensure that DA commitments ($P^{DA}_{t,\omega}$) respect the physical power exchange limit $\overline{P}^{\text{POI}}$ at the plant's point of interconnection (POI). This limits speculative behavior by preventing the plant from committing unrealistic DA purchases based on expected DA–RT price spreads.

$$\Delta P^{\updownarrow}_{t,\omega} = P^{\text{POI,RT}}_{t,\omega} - P^{DA}_{t,\omega} \qquad \forall t\in T, \forall\omega\in\Omega_\omega \tag{4}$$

$$\Delta P^{I}_{t,\omega} \ge \pm(P^{\text{POI,RT}}_{t,\omega} - P^{DA}_{t,\omega}) \qquad \forall t\in T, \forall\omega\in\Omega_\omega \tag{5}$$

$$P^{DA}_{t,\omega} \le \overline{P}^{\text{POI}} \qquad \forall t\in T, \forall\omega\in\Omega_\omega \tag{6}$$

From the assets perspective, on-site RG production ($P_{r,t,\omega}$) reduces the net load of the plant, but its available power ($\overline{P}_{r,t,\omega}$) is subject to real-time uncertainty:

979-8-3315-8138-1

$$0 \leq P_{r,t,\omega} \leq \overline{P}_{r,t,\omega} \quad \forall r \in R, \forall t \in T, \forall \omega \in \Omega_\omega \tag{7}$$

The BESS dynamics is captured by the energy balance below, which accounts for charging (η_b^{ch}) and discharging (η_b^{dch}) efficiencies, self-discharge losses (σ_b^{self}), and FCR reserve activations ($\Delta P_{b,t,\omega}^{R,ch}$ and $\Delta P_{b,t,\omega}^{R,dch}$).

$$E_{b,t+1,\omega} = E_{b,t,\omega} + \Bigg((P_{b,t,\omega}^{ch} + \Delta P_{b,t,\omega}^{R,ch})\eta_b^{ch} - \frac{(P_{b,t,\omega}^{dch} + \Delta P_{b,t,\omega}^{R,dch})}{\eta_b^{dch}} \Bigg)\Delta t - \sigma_b^{self} \quad \forall b \in B, \forall t \in T, \forall \omega \in \Omega_\omega \tag{8}$$

$$E_{b,0,\omega} = E_b^{ini} \quad \forall b \in B, \forall \omega \in \Omega_\omega \tag{9}$$

$$E_b^{rated}\underline{SOC}_b \leq E_{b,t,\omega} \leq E_b^{rated}\overline{SOC}_b \quad \forall b \in B, \forall t \in T, \forall \omega \in \Omega_\omega \tag{10}$$

$$0 \leq P_{b,t,\omega}^{ch} + P_{b,t,\omega}^{R,FCR,ch} \leq \overline{P}_b^{ch} x_{b,t,\omega} \quad \forall b \in B, \forall t \in T, \forall \omega \in \Omega_\omega \tag{11}$$

$$0 \leq P_{b,t,\omega}^{dch} + P_{b,t,\omega}^{R,FCR,dch} \leq \overline{P}_b^{dch}(1 - x_{b,t,\omega}) \quad \forall b \in B, \forall t \in T, \forall \omega \in \Omega_\omega \tag{12}$$

FCR reserves are split into charging and discharging components to enable bidirectional droop activation, although a single FCR capacity $P_{b,t,\omega}^{R,FCR}$ is committed in the first stage, equal to the sum of both components. To ensure sufficient energy headroom, SOC margins are included in constraints (13) and (14). These margins encourage the model to maintain available energy capacity even when no activation is expected, where α^{FCR} denotes the ratio of power capacity allocated to SOC headroom, and $\delta^{\text{SOC,-}}$ and $\delta^{\text{SOC,+}}$ are slack variables penalized in Eq. (1).

$$E_{b,t,\omega} \leq E_b^{rated}\overline{SOC}_b - \alpha^{\text{FCR}} P_{b,t,\omega}^{R,FCR}\eta_b^{ch} + \delta_{b,t,\omega}^{\text{SOC,+}} \quad \forall b \in B, \forall t \in T, \forall \omega \in \Omega_\omega \tag{13}$$

$$E_{b,t,\omega} \geq E_b^{rated}\underline{SOC}_b + \alpha^{\text{FCR}} \frac{P_{b,t,\omega}^{R,FCR}}{\eta_b^{dch}} - \delta_{b,t,\omega}^{\text{SOC,-}} \quad \forall b \in B, \forall t \in T, \forall \omega \in \Omega_\omega \tag{14}$$

The active power consumption of dispatchable machines is regulated discretely as a function of electrical efficiency (η_p^{el}), rated throughput ($\overline{F}_p$), and a binary ON/OFF variable ($\mu_{p,t,\omega}$), as shown in constraint (15). The latter is a third-stage decision, determined after the realization of DA prices and before real-time operation. Real-time mFRR activation is represented in constraint (16) as the product of a binary activation factor ($y_{t,\omega}^{\text{act,mFRR}}$) and the sum of committed mFRR capacities. The activation factor is modeled by building on the method proposed in [9], assuming activation occurs only when the expected system-level activation meets or exceeds the available mFRR potential. Consequently, real-time power consumption deviates from the scheduled one for mFRR-capable machines, as shown in constraint (17).

$$P_{p,t,\omega} = \eta_p^{el}\,\overline{F}_p\,\mu_{p,t,\omega}, \quad \forall p \in \mathcal{P},\ \forall t \in T,\ \forall \omega \in \Omega_\omega \tag{15}$$

$$\sum_m P_{m,t,\omega}^{\text{act,mFRR}} = y_{t,\omega}^{\text{act,mFRR}} \sum_m P_{m,t,\omega}^{\text{R,mFRR}} \quad \forall t \in T,\ \forall \omega \in \Omega_\omega \tag{16}$$

$$P_{p,t,\omega}^{\text{RT}} = \begin{cases} P_{p,t,\omega} - P_{M(p),t,\omega}^{\text{act,mFRR}}, & \forall p \in \mathcal{P}^{\text{mFRR}}, \forall t \in T, \forall \omega \in \Omega_\omega \\ P_{p,t,\omega}, & \forall p \in \mathcal{P} \setminus \mathcal{P}^{\text{mFRR}}, \forall t \in T, \forall \omega \in \Omega_\omega \end{cases} \tag{17}$$

Scheduled switching actions are subject to the minimum on/off time requirements defined in constraints (18) and (19). These constraints limit the duration that each process must remain in a given state after a state transition, controlled by parameters α_p^{on} and α_p^{off}.

$$(\mu_{p,t+1,\omega} - \mu_{p,t,\omega})\,\alpha_p^{\text{on}} \leq \sum_{j=1}^{\alpha_p^{\text{on}}} \mu_{p,(t+j),\omega} \quad \forall p \in \mathcal{P}, \forall t \in T_{\text{on}}, \forall \omega \in \Omega_\omega \tag{18}$$

$$(1 + \mu_{p,t+1,\omega} - \mu_{p,t,\omega})\,\alpha_p^{\text{off}} \leq \sum_{j=1}^{\alpha_p^{\text{off}}} \mu_{p,(t+j),\omega} \quad \forall p \in \mathcal{P}, \forall t \in T_{\text{off}}, \forall \omega \in \Omega_\omega \tag{19}$$

Inventory dynamics are modeled through material balance equations (20) and (21) that link upstream and downstream processes. Material levels are affected by inflows and outflows, which may include cement demand F^{dem}, as in contraint (21).

$$M_{s,t+1,\omega} = M_{s,t,\omega} + \Delta t\Bigg(\sum_{p1 \in \omega_s^U} \overline{F}_{p1}\mu_{p1,t,\omega} - \sum_{p2 \in \omega_s^D} \eta_{p2}^{mat}\overline{F}_{p2}\mu_{p2,t,\omega} \Bigg) \quad \forall s \in S \setminus S_D, \quad \forall t \in T, \quad \forall \omega \in \Omega_\omega \tag{20}$$

$$M_{s,t+1,\omega} = M_{s,t,\omega} + \Delta t\Bigg(\sum_{p1 \in \omega_s^U} \overline{F}_{p1}\mu_{p1,t,\omega} - F_t^{dem} \Bigg) \quad \forall s \in S_D, \quad \forall t \in T, \quad \forall \omega \in \Omega_\omega \tag{21}$$

$$M_{s,0,\omega} = M_s^{ini} \quad \forall s \in S, \forall \omega \in \Omega_\omega \tag{22}$$

$$\underline{M}_s \leq M_{s,t,\omega} \leq \overline{M}_s \quad \forall s \in S, \forall t \in T, \forall \omega \in \Omega_\omega \tag{23}$$

Real-time inventories are differentiated from scheduled ones for material streams connected to mFRR-capable processes, reflecting potential deviations caused by reserve activation upstream ($\Delta^{\text{up}}_{s,t,\omega} = -\sum_{p1\in\omega^{U}_{s}\cap\mathcal{P}^{\text{mFRR}}} \frac{P^{\text{act,mFRR}}_{p1,t,\omega}}{\eta^{\text{el}}_{p}}$) or downstream ($\Delta^{\text{down}}_{s,t,\omega} = \sum_{p2\in\omega^{D}_{s}\cap\mathcal{P}^{\text{mFRR}}} \eta^{mat}_{p2} \frac{P^{\text{act,mFRR}}_{p2,t,\omega}}{\eta^{\text{el}}_{p}}$) of a given inventory. Constraint (26) is a soft constraint that penalize deviations from end-of-horizon target levels in the objective function.

$$M^{\text{RT}}_{s,t+1,\omega} - M_{s,t+1,\omega} = \left(M^{\text{RT}}_{s,t,\omega} - M_{s,t,\omega}\right) + \Delta t \cdot \left(\Delta^{\text{up}}_{s,t,\omega} + \Delta^{\text{down}}_{s,t,\omega}\right) \quad \forall s \in S, \forall t \in T, \forall \omega \in \Omega_\omega \tag{24}$$

$$P^{\text{R,mFRR}}_{M(p),t,\omega} \leq P_{p,t,\omega} \quad \forall p \in \mathcal{P}^{\text{mFRR}},\ \forall t \in T,\ \forall \omega \in \Omega_\omega \tag{25}$$

$$M^{target}_{s} - \delta^{\text{M,-}}_{s,\omega} \leq M^{\text{RT}}_{s,t_f+1,\omega} \leq M^{target}_{s} + \delta^{\text{M,+}}_{s,\omega} \quad \forall s \in S, \forall \omega \in \Omega_\omega \tag{26}$$

Finally, the real-time power balance is formulated under a copper-plate assumption (i.e., assets are connected to a single node), accounting for all internal power injections (negative terms) and absorptions (positive terms) within the plant:

$$P^{\text{POI,RT}}_{t,\omega} = -\sum_{r\in R} P_{r,t,\omega} - \sum_{b\in B} \Big((P^{dch}_{b,t,\omega} + \Delta P^{R,dch}_{b,t,\omega}) - (P^{ch}_{b,t,\omega} + \Delta P^{R,ch}_{b,t,\omega}) \Big) + \sum_{d\in D} P_{d,t} + \sum_{p\in\mathcal{P}} P^{\text{RT}}_{p,t,\omega} \quad \forall t \in T, \forall \omega \in \Omega_\omega \tag{27}$$

D. Scenario generation and rolling-horizon simulation

A stagewise sequential clustering approach is employed to represent uncertainty, generating a scenario tree whose nodes correspond to clusters at each decision stage. Historical data are grouped using K-medoids clustering to capture representative realizations of uncertain parameters. In the first stage, FCR and mFRR capacity prices are jointly clustered according to the specified number of clusters. In the second stage, DA prices are clustered conditionally on the reserve clusters to preserve inter-stage dependencies. Finally, RT parameters—including activation signals, balancing prices, and RG—are clustered based on the corresponding DA clusters. To control tree size and avoid branches with insufficient data, an adaptive clustering procedure reduces the number of clusters when the available samples fall below a threshold.

A rolling-horizon simulation is conducted to evaluate how in-sample stochastic policies perform under out-of-sample realizations and to track cumulative inventory deviations. The procedure is summarized in Algorithm 1.

Algorithm 1 Rolling-horizon simulation procedure

Input: Total days D, horizon H=24 h, initial state s_1=$(M_0, \text{SOC}_0, \text{ON/OFF}_0)$

for $d = 1, \ldots, D$ **do**
- Generate scenario set Ω_d from lookback window $[d{-}N, \ldots, d{-}1]$
- Minimize Eq. (1) for day d to obtain optimal policy x_d
- Map in-sample scenarios to realized outcomes via nearest-distance rule
- Apply mapped policy $x^{\star}_{d}$ to out-of-sample trajectory
- Update next day state s_{d+1} $(M_f, \text{SOC}_f, \text{ON/OFF}_f)$

Return: Aggregated in- and out-of-sample cost

III. Case study

The rolling-horizon simulation spans 21 June–28 August 2021, covering over two months of operation for a representative cement plant in the DK1 bidding zone. The year is chosen due to data availability on mFRR activations and grid frequency. Market and renewable data are sourced from Energinet [10], and frequency data from WETI [11]. mFRR activations are modeled with hourly resolution, consistent with available data [12]. The plant operates at 200 ton/h, with equipment sized from typical throughput data [5], and includes on-site PV (20 MW), wind (30 MW), and BESS (10 MW/30 MWh). For the simulations, the following input cluster numbers are set: 2 for FCR data, 3 for DA data, and 4 for RT data. This results in 24 scenarios if the adaptive clustering does not limit branching. Moreover, a 45-day lookback window is employed.

Performance is benchmarked against deterministic and perfect-foresight cases; the former optimizes a single average scenario, while the latter optimizes decisions using realized out-of-sample data, representing an ideal upper bound.

A. Results and discussion

Fig. 2 compares the first days of operation for the stochastic and deterministic models, considering participation in all market layers described in Section II. In the stochastic model, process scheduling accounts for multiple price and activation scenarios, leading to more cautious and less frequent mFRR reserve commitments. Following an activation event (e.g., 26–27 June), the model prioritizes inventory recovery, temporarily suspending reserve bids. In contrast, the deterministic model optimizes for a single expected scenario, neglecting uncertainty and resulting in an overconfident mFRR bidding strategy. Without uncertainty representation, cumulative activations hinder inventory recovery, as the model overestimates its ability to restore material levels while earning from reserve capacity. Thus, operation becomes infeasible after 26 June, when the calcined clay inventory exceeds its 2000 ton limit.

Table I summarizes total market costs and savings for three participation cases: Energy-only, FCR-only, and FCR & mFRR. The Energy-only case serves as the baseline for computing cost savings within each simulation type. Here, cost differences mainly stem from scheduling arbitrage and strategic bidding: under perfect foresight, where day-ahead and real-time prices are known, the optimizer deliberately under- or overcommits bids to exploit price spreads. Allowing the BESS to provide FCR (up to 10 MW) yields savings of 3–6 %. Although the deterministic formulation shows slightly higher relative savings, it has marginally higher absolute costs than

979-8-3315-8138-1

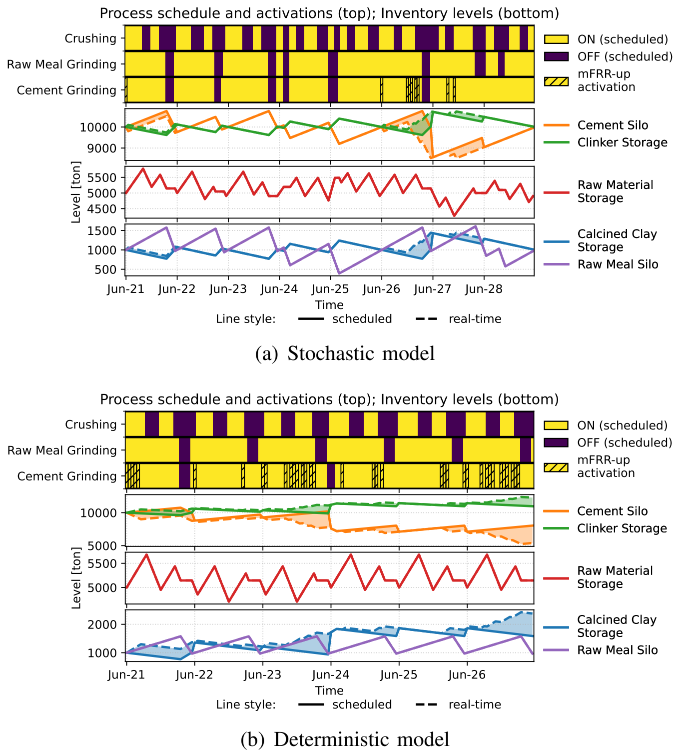

(a) Stochastic model

(b) Deterministic model

Fig. 2. Impact of mFRR activations on production and inventories: (a) stochastic and (b) deterministic model. Shaded areas show deviations between scheduled and real-time inventory levels. Rated powers: 0.39 MW (crushing), 1.8 MW (raw meal grinding), 7.9 MW (cement grinding).

the stochastic one because savings are calculated with respect to the same simulation type. The gap between stochastic and perfect-foresight solutions is around 1 M€, highlighting the value of perfect information.

Introducing mFRR bidding (7.9 MW capacity) increases operational complexity due to activation uncertainty, which may push inventories beyond physical limits if neglected (see Fig. 2). Stochastic savings rise from 3.0 % to 3.9 % (≈ 40 k€) when mFRR provision is allowed—roughly one-third of the gains achieved with FCR alone. This smaller benefit reflects higher FCR capacity prices compared to mFRR during the analyzed period. Although mFRR activations can yield revenues, they are highly uncertain in both activation and price and often trigger rebound effects that raise subsequent energy costs. Under perfect foresight, potential savings increase by about 1.2 M€ relative to the stochastic case.

Overall, the stochastic formulation's main advantage lies less in cost reduction and more in its ability to manage activation uncertainty and maintain feasible production–inventory trajectories, particularly in the FCR & mFRR case.

IV. Conclusions

This paper presents a multi-stage stochastic optimization model for co-optimizing energy and ancillary service procurement for a cement plant under uncertainty. A rolling-horizon simulation with out-of-sample evaluation is used to assess the cumulative impact of mFRR activations on plant

TABLE I
Total market cost and savings vs energy-only baseline.

Case	Simulation	Cost [M€]	Savings [%]
Energy-only	*Deterministic*	4.11	–
	Stochastic	4.07	–
	Perfect foresight	3.16	–
FCR-only	*Deterministic*	3.97	3.27
	Stochastic	3.95	2.98
	Perfect foresight	2.95	6.65
mFRR & FCR	*Deterministic*	Infeasible	Infeasible
	Stochastic	3.91	3.95
	Perfect foresight	2.74	13.31

operation. The results emphasize the importance of uncertainty characterization, particularly when modelling energy-intensive services such as mFRR, whose activations have a significant impact on short-term production and inventory planning. In contrast, non-energy-intensive services such as FCR yield cost reductions that are less sensitive to uncertainty modelling but depend on on-site BESS investments. Future work will integrate a risk-averse formulation, extend the optimization horizon, and conduct sensitivity analyses on key parameters.

References

[1] H. Golmohamadi, "Demand-side management in industrial sector: A review of heavy industries," *Renew. Sustain. Energy Rev.*, vol. 156, p. 111963, 2022.

[2] M. H. Shoreh, P. Siano, M. Shafie-khah, V. Loia, and J. P. Catalão, "A survey of industrial applications of demand response," *Electr. Power Syst. Res.*, vol. 141, pp. 31–49, 2016.

[3] J. A. Swanepoel, E. H. Mathews, J. Vosloo, and L. Liebenberg, "Integrated energy optimisation for the cement industry: A case study perspective," *Energy Conversion and Management*, vol. 78, pp. 765–775, 2014.

[4] D. L. Summerbell, D. Khripko, C. Barlow, and J. Hesselbach, "Cost and carbon reductions from industrial demand-side management: Study of potential savings at a cement plant," *Applied Energy*, vol. 197, pp. 100–113, 2017.

[5] A. T. Mossie, D. Khatiwada, B. Palm, and G. Bekele, "Energy demand flexibility potential in cement industries: How does it contribute to energy supply security and environmental sustainability?," *Appl. Energy*, vol. 377, p. 124608, 2025.

[6] M. Bohlayer, M. Fleschutz, M. Braun, and G. Zöttl, "Energy-intense production-inventory planning with participation in sequential energy markets," *Appl. Energy*, vol. 258, p. 113954, 2020.

[7] J. Arellano, García-Cerezo, and M. Carrión, "Optimal participation in manual frequency restoration reserve-based demand response programs for large consumers," *IEEE Access*, vol. 13, pp. 59866–59885, 2025.

[8] K. Scrivener, F. Martirena, S. Bishnoi, and S. Maity, "Calcined clay limestone cements (lc3)," *Cem. Concr. Res.*, vol. 114, pp. 49–56, 2018.

[9] B. Crowley, S. E. C. Magid, D. B. V. Nielsen, J. Shin, and A. S. Skak-Iversen, "Can energy communities provide ancillary services? a stochastic program for aggregated bidding in the nordic ancillary markets," in *2024 IEEE International Conference on Communications, Control, and Computing Technologies for Smart Grids (SmartGridComm)*, pp. 283–288, Sep. 2024.

[10] Energinet, "Energi data service," 2025. Accessed: Jan. 29, 2025.

[11] H. Thiesen, C. Jauch, and A. Gloe, "Grid frequency data - weti," 2021. Last updated: Jan. 8, 2023. License: CC-By Attribution 4.0 International. Accessed: Jan. 29, 2025.

[12] A. G. Johnsen, L. Mitridati, D. Zarrilli, and J. Kazempour, "The value of ancillary services for electrolyzers," *Computers Chemical Engineering*, vol. 204, p. 109360, 2026.

979-8-3315-8138-1